Received: 18 July 2021 | Revised: 11 April 2022 | Accepted: 10 July 2022
DOI: 10.1002/we.2772

RESEARCH ARTICLE

WILEY

Assessment of an actuator disk-based approach for the prediction of fatigue loads in a perspective of wind farm-scale application

Maud Moens | Matthieu Duponcheel | Philippe Chatelain

Institute of Mechanics, Materials and Civil Engineering, Université catholique de Louvain, Louvain-la-Neuve, Belgium

Correspondence
Maud Moens, Institute of Mechanics, Materials and Civil Engineering, Université catholique de Louvain, 1348 Louvain-la-Neuve, Belgium.
Email: maud.moens@uclouvain.be

Funding information
European Union's Horizon 2020 research and innovation program, Grant/Award Number: 725627

Abstract

This work aims at assessing the loads and the fatigue estimates computed using an advanced actuator disk (AD) method coupled to large eddy simulation, at a resolution appropriate for large wind farm calculations. In order to compute pertinent fatigue loads, blade trajectories are replicated through the disk, and the AD aerodynamic forces are interpolated onto these "virtual blades" at each time step. This approach, denoted AD-B, is verified against a Vortex-Particle Mesh (VPM) method coupled to immersed lifting lines at a fine resolution, through simulations of an isolated rotor in a turbulent wind. Two different methods are used to evaluate the fatigue damages: the widely used Rainflow counting (RFC) procedure and the spectral Dirlik's approach (DK), both combined with a Palgrem–Miner rule. In the present work, the DK counting method is considered to further investigate the potential of extrapolating some loading data in the high frequencies, uncaptured by the AD-B model at a coarse resolution. The results show that the fatigue estimates computed using the RFC procedure are very similar for the VPM and the AD-B methods, thus without any modeling of the unresolved scales for the disk. Indeed, the AD-B model captures the loads of middle and large amplitudes that contribute the most to the rotor damage. The use of extrapolated loading data makes the AD-B fatigue estimates closer to the VPM ones, but the DK counting method globally leads to results that are quite different from those obtained using the RFC procedure. Further investigations are thus required for the combination of extrapolated loading information and spectral counting methods.

KEYWORDS
actuator disk, fatigue loads, large eddy simulation, Rainflow counting, spectral counting method

1 | INTRODUCTION

Fatigue is a critical factor in the lifetime of a wind turbine and is one of the causes of failure of the machine components.[1] The actual loads that contribute to fatigue of a wind turbine originate from a variety of sources: high winds, wind shear, gravity and/or potential yaw errors, turbulent

This is an open access article under the terms of the Creative Commons Attribution-NonCommercial-NoDerivs License, which permits use and distribution in any medium, provided the original work is properly cited, the use is non-commercial and no modifications or adaptations are made.
© 2022 The Authors. *Wind Energy* published by John Wiley & Sons Ltd.

fluctuations, ambient gusts, starts and stops of the machine, and so on. Moreover, in a wind farm arrangement, fatigue phenomenon is exacerbated by the presence of other rotors: The wind turbines impacted by the wake of the upstream machines see their cumulated fatigue damage rise due to the increase level of ambient turbulence and the wake meandering phenomenon. The variety of these load sources and the complexity of some of them increase the uncertainties in the predicted fatigue damage, leading to unexpected failures for some wind turbine components. For some wind turbine subassemblies, the downtime associated with repair may be significant, mainly in the offshore environment: This decreases the wind turbine reliability, directly impacting the Levelized Cost of Energy, as demonstrated in Dao et al.[2]

It is thus of a crucial importance to deploy efforts in the prediction of the fatigue damage a wind turbine will suffer during its operation, either to optimally design the wind farm or to develop load alleviation strategies that can be used during the wind farm operation. Those strategies encompass load alleviation at a wind turbine level[3–5] but also schemes aiming at ensuring a more uniform and potentially reduced wear and tear of the rotors at a wind farm scale.[6,7]

As the development of control strategies or the potential arrangement of a future wind farm often relies on numerical studies, it is essential that the simulation tools provide accurate blade/structural loads and fatigue estimates. Moreover, more and more control strategies use information coming from blade bending moments and structural loads for estimating relevant characteristics of the wind turbine environment. These sensing technologies aim at characterizing the incoming wind[8] or predicting the wake behavior downstream of the machines,[9,10] through surrogate wake models in particular.[11] This reinforces the requirement of accurate virtual wind farm environments in which the control schemes can be developed and tested.

Several numerical methods that capture fatigue loads at a wind farm scale exist, and their use depends on the considered application. Lower fidelity approaches, usually implying a Blade Element Momentum (BEM) method combined to a wake model, are often used to evaluate the fatigue damage for the wind farm lifetime. Indeed, their low computational costs allow simulations that cover all the incoming wind speeds and directions that a wind farm will meet during its operation. The BEM approach has already demonstrated its performances to accurately represent the wind turbine behavior, even immersed in a complex turbulent inflow,[12] and its coupling to an aero elastic code allows to perform accurate fatigue loads investigations.[13,14] Its combination to wake models that capture the unsteady wake behavior while remaining computationally inexpensive allows to extend the studies at the scale of a wind farm. For example, Larsen et al.[15] validated a numerical approach based on a Dynamic Wake Meandering (DWM) model[16] and a BEM implemented in the aeroelastic code HAWC2, by comparing the fatigue loads of one turbine within the Egmond aan Zee wind farm to actual measurements. Galinos et al.[17] used the same method for computing the representative 20-year lifetime fatigue loads and power production for the Horns Rev wind farm. Schmidt et al.[18] also investigated the fatigue loads for one machine inside the Horns Rev wind farm, using the DWM implemented into GH Bladed. Those fast approaches or variants of them were also used to investigate control strategies that account for fatigue loads.[19–22] Thanks to their efficiency, the approaches described above are also particularly suitable for model based control, allowing the prediction of the wind turbine fatigue loads and wake behavior and a more accurate control.

Although the DWM model used in several of these approaches accounts for the wake meandering, it remains of medium fidelity, and it cannot capture all the fine physics arising of the complex wake flow phenomena (e.g., wake merging or wake destructuration). If we want to have a high-fidelity virtual environment in which we can study fatigue loads in more detail, test the global control strategies, or verify/validate the low and medium fidelity approaches described above, we have to increase the accuracy of the numerical tool. Large eddy simulation (LES) coupled to a wind turbine model is currently one of the most appropriate approaches for an accurate and efficient representation of a wind farm. Indeed, LES intrinsically and accurately captures unsteady effects and thus the complex wake phenomena that contribute for a significant part of the fatigue damage. For example, LES, coupled with an actuator line (AL) approach for the wind turbine model, was used in several numerical studies for investigating fatigue loads and damages. Lee et al.[23] investigated fatigue loads for two floating wind turbines, with the second machine located in the wake of the first one. The flow solver was two-way coupled with the aeroelastic code FAST.[24] Liu et al.[25] also considered fatigue damages for a tandem of wind turbines, but the AL method was only adopted for the first wind turbine, in order to simulate the wake flow field numerically. The fatigue loads of the downstream rotor were thus computed using an aeroelastic tool coupled to a BEM method. Meng et al.[26] studied the fatigue damages through a small wind farm with nine wind turbines, modeled using an aeroelastic AL method. Churchfield et al.[27] performed LES of 36 wind turbines in order to compare the fatigue loads of some machines to those obtained using the DWM model coupled to FAST[24] and those available from measurements.

We see that most of studies considered a limited number of rotors or simulations, as the AL method requires fine spatio-temporal resolutions. Simulating very large wind farms imposes a coarsening of the resolution, in order to keep the computation cost acceptable. The use of an actuator disk (AD) approach for modeling the rotor behavior thus appears as the most relevant procedure: With this model, the actual geometry of rotor blades is replaced by a regularized body force term acting over the surface swept by the blades. There are different levels of fidelity for the AD approaches, and the most advanced models include torque effects and force computations based on the prevailing velocities at the disk location.[28–30] This last feature allows the wind turbine model to capture temporal and spatial rotor loads variations, which could give relevant information about blade loading and bending moments. However, compared to discrete line type approaches, for which it is trivial to know the instantaneous blade loading and thus, the root bending moments, the AD method distributes the effect of blades all over the disk. In order to reproduce pertinent loads, a possible approach consists of replicating the blade trajectories through the disk and interpolate the AD aerodynamic forces onto these "virtual blades" at each time step. It is thus possible to integrate the aerodynamic forces along the blades and to easily recover

10991824, 2022, 11, Downloaded from https://onlinelibrary.wiley.com/doi/10.1002/we.2772 by Bibliothecaire En Chef Uni Catholique De Louvain (Ucl), Wiley Online Library on [18/03/2024]. See the Terms and Conditions (https://onlinelibrary.wiley.com/terms-and-conditions) on Wiley Online Library for rules of use; OA articles are governed by the applicable Creative Commons License

fatigue loads, as in a discrete line type approach. There are very few results in the literature for the mentioned approach: This method has been used in Martinen et al.[31] for estimating fatigue loads from an AD, for two aligned and curtailed wind turbines. However, there was a lack of verification of the method itself, and the AD approach was used at a quite fine resolution (31 points per radius), which is computationally unaffordable at a large wind farm scale. It is thus very relevant to verify the fatigue estimates recovered from an AD model at coarser resolutions.

The present study aims at assessing fatigue loads of an isolated rotor computed with an AD approach at such particular resolutions, by comparing them to those obtained with a discrete line type approach at a very fine resolution. For estimating the fatigue damages, we consider a rainflow counting (RFC) method[32] combined with a Palmgren–Miner[33] rule. This is the most widespread procedure used in the wind energy sector, for determining the lifetime of the rotor components for potential installations.[34,35] This approach is also used in many research works, for investigating loads either from on-site measurements[36,37] or from numerical studies.[23,25] The RFC procedure counts the number of load cycles based on the temporal signals. Another type of approach estimates the fatigue damage in the frequency domain, by obtaining information equivalent to cycle counts directly from the one-sided power spectrum density (PSD) of the load fluctuations.[38] This procedure is mainly used in offshore and automative industries, to avoid extensive simulation or measurement campaigns required for performing an accurate RFC method. In the present work, such an approach is considered to further investigate the potential of extrapolating some loading data of the PSD. This will aim at recovering relevant fatigue information linked to the smallest flow scales, which simply cannot be captured by an AD model at a coarse resolution. We here consider the Dirlik's spectral method,[39] as several research works showed that it led to the most accurate fatigue estimates for wind turbine components.[36,40–42]

The flow solvers, the wind turbine models, and the methods for recovering the fatigue loads and computing fatigue damages are described in Section 2. Section 3 reports the configuration and the generation of the inflow wind. We here consider an isolated wind turbine impacted by a turbulent wind at several operating conditions. The investigations of the fatigue loads and the comparison of the fatigue damage estimates are presented in Section 4. Our conclusions are finally drawn in Section 5.

2 | METHOD

2.1 | Fourth-order finite difference flow solver and AD model

We consider the LES of incompressible flows. It is performed using an in-house fourth-order finite difference (FD4) code,[43] formulated in primitive variables (i.e., in velocity and pressure) and using a staggered mesh arrangement. Details about the code and the main equations can be found in Moens et al.[30] In the present study, the subgrid scale model is a regularized variational multiscale (RVM) variant[44] of the classical Smagorinsky model.[45] The wind turbine is added through external body force terms (per unit volume) acting on the flow.

The inlet boundary condition is a constant wind speed, over which turbulent fluctuations are imposed (the generation of the turbulence is discussed in Section 3). A natural convective boundary condition is applied at the outflow, and periodic boundary conditions are used in the lateral and vertical directions. All the meshes used in the present work are uniform and do not involve local refinement in the rotor region or in its wake.

2.1.1 | AD model

The AD approach of Moens et al.[30] is used here. It is a rotating AD for which the aerodynamic forces are estimated from local velocities and improved with a tip-loss factor. In Moens et al.,[30] this AD model, used at a coarse resolution, was verified with a higher fidelity approach at a finer resolution, the Vortex Particle-Mesh (VPM) method coupled to immersed lifting lines (LLs). We here briefly recall the methodology.

The disk is discretized into a certain number of elements in both radial and azimuthal directions (see Figure 1A). On each small disk surface, we account for the N_b blades aerodynamic forces. Those are governed by the local velocities, that is, the normal and tangential velocities to the rotor plane, u_n and u_θ, respectively, and determined from the 2-D airfoil characteristics, that is, the lift and drag coefficients, C_l and C_d, the chord length, c, the blade twist, β, and the possible pitch angle of the blade, γ. Figure 1B presents the velocities and forces at a location r on the blade: u_θ is the velocity induced by the wake in the tangential direction, while u_n represents the difference between the upstream velocity and the velocity induced by the wake in the normal direction. u_n and u_θ are recovered from the flow solver and corrected with a tip-loss correction before their use in the computation of the forces (see Moens et al.[30] for details of this correction).

The lift and drag aerodynamic forces per blade length Δr are thus computed as

$$\begin{pmatrix} L \\ D \end{pmatrix} = 0.5\rho V_{rel}^2 c \begin{pmatrix} C_l \\ C_d \end{pmatrix} \tag{1}$$

with V_{rel} the relative velocity magnitude:

10991824, 2022, 11, Downloaded from https://onlinelibrary.wiley.com/doi/10.1002/we.2772 by Bibliothecaire En Chef Uni Catholique De Louvain (Ucl), Wiley Online Library on [18/03/2024]. See the Terms and Conditions (https://onlinelibrary.wiley.com/terms-and-conditions) on Wiley Online Library for rules of use; OA articles are governed by the applicable Creative Commons License

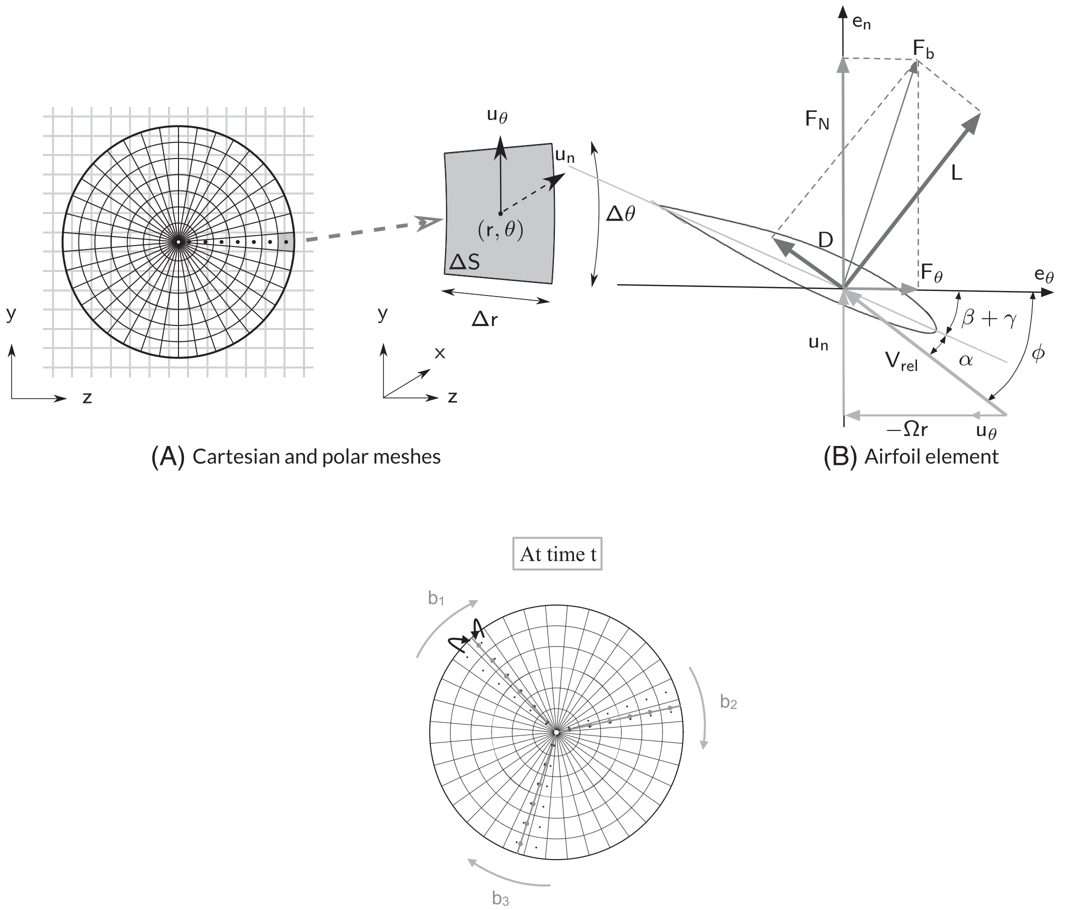

(A) Cartesian and polar meshes

(B) Airfoil element

(C) AD-B model: the AD forces are interpolated on the virtual blades b_i

FIGURE 1 Schematics of meshes, AD methods, and blade airfoil; definition of the vector quantities and notations

$$V_{rel} = \sqrt{u_n^2 + (\Omega r - u_\theta)^2}. \tag{2}$$

(C_l, C_d) are obtained from the effective angle of attack α and tabulated 2D airfoil data; α is computed from the difference between the flow angle, $\phi = \arctan(u_n/(\Omega r - u_\theta))$, and the sum of the twist and pitch angles, β and γ; Ω is the rotor speed. L and D are then expressed in the normal and tangential directions of the disk plane (see Figure 1B),

$$F_N = L\cos\phi + D\sin\phi \quad \text{and} \quad F_\theta = L\sin\phi - D\cos\phi\,, \tag{3}$$

and F_N and F_θ are finally multiplied by the number of blades N_b, the blade section length Δr, and a weight that corresponds to the ratio between the surface element ΔS and the total annular surface at the given radius r,

$$F_{N,AD} = N_b F_N \Delta r \frac{\Delta S}{2\pi r \Delta r} \quad \text{and} \quad F_{\theta,AD} = N_b F_\theta \Delta r \frac{\Delta S}{2\pi r \Delta r}. \tag{4}$$

These forces are finally translated into bulk forces for the LES equations by using the M_4 kernel,[46] a second-order mollifier.

By integrating the forces distribution, diagnostics can be computed, such as the thrust, T, the torque, Q, and the power, $P = \Omega Q$.

10991824, 2022, 11, Downloaded from https://onlinelibrary.wiley.com/doi/10.1002/we.2772 by Bibliothecaire En Chef Uni Catholique De Louvain (Ucl), Wiley Online Library on [18/03/2024]. See the Terms and Conditions (https://onlinelibrary.wiley.com/terms-and-conditions) on Wiley Online Library for rules of use; OA articles are governed by the applicable Creative Commons License

2.2 | VPM flow solver and lifting lines

In order to verify the AD approach and to assess the estimation of fatigue loads, the AD simulations are compared to higher fidelity calculations of a classical three-bladed rotor. The reference computations are performed using a VPM method coupled to immersed LLs.[47,48] It relies on the Lagrangian discretization of the Navier–Stokes equations in vorticity–velocity formulation, where advection is handled by the particles and the mesh allows the evaluation of the differential operators and the use of a fast Poisson solver. The use of a Fourier-based Poisson solver here allows for transverse unbounded directions and inlet/outlet boundaries.[47] The advection being handled by the particles, the method exhibits little dissipation and dispersion errors and achieves high accuracy in computations of turbulent flows such as a wind turbine wake.[48] The generation of vorticity along the blades is accounted for through a LL model: With this approach, the flow is assumed to be two-dimensional past airfoil sections along the blade. The produced lift can be obtained from aerodynamic data (lift coefficients of the airfoils, velocity at the blade, …) and used in the Kutta–Joukowsky theorem to obtain the circulation attached to the blade. The spanwise and temporal changes in the bound circulation give rise to the shedding of vortex sheets in a fashion akin to a Vortex Lattice method; those roll up and coalesce into a developed wake. For additional details and representative examples of the method, we refer to Caprace et al. and Balty et al.[49,50]

2.3 | Estimation of the fatigue loads

In this paper, we consider the blade root bending moments, that is, the flapwise and the edgewise moments, and the rotor yaw and tilt moments. We only consider the aerodynamic contributions to these moments. Other contributions, such as gravity loading, are not included in the present investigation.

The flapwise and edgewise moments per blade b are denoted $M_{f,b}$ and $M_{e,b}$, respectively, and are evaluated as

$$M_{f,b} = \int_{R_{hub}}^{R_{tip}} (r - R_{hub}) \mathbf{F_b} . \mathbf{e_n} \, dr \, , \tag{5}$$

$$M_{e,b} = \int_{R_{hub}}^{R_{tip}} (r\text{-}R_{hub}) \, \mathbf{F_b} . \mathbf{e}_\theta \, dr, \tag{6}$$

where $\mathbf{F_b}$ is the aerodynamic blade force per length; $\mathbf{e_n}$ and $\mathbf{e}_\theta$ are the unit vectors normal and tangential to the rotor plane, respectively (see Figure 1B); R_{hub} and R_{tip} are the radii at the hub and the tip locations. The yawing and the tilting moments, denoted M_y and M_t, respectively, are expressed as

$$M_y = \sum_{b=1}^{N_b} \mathbf{e_y} \, . \int_{R_{hub}}^{R_{tip}} \mathbf{x} \times \mathbf{F_b} \, dr \, , \tag{7}$$

$$M_t = \sum_{b=1}^{N_b} \mathbf{e_z} \, . \int_{R_{hub}}^{R_{tip}} \mathbf{x} \times \mathbf{F_b} \, dr \, , \tag{8}$$

where N_b is the number of blades; $\mathbf{x}$ is the position from the hub center and the considered force point; $\mathbf{e_y}$ and $\mathbf{e_z}$ correspond the yaw and tilt axes, respectively. In the present study, only the normal force component plays a role in the yaw and tilt moments.

For discrete line type approaches, such as the LL method, the instantaneous blade loading is directly available and can be integrated along the blade span. For the AD method, we propose to replicate the blade trajectories through the disk and recompute blade-attached aerodynamic forces. At each particular radial position, r, and time, t, the forces acting on the blade b, $F_{b,N}$ and $F_{b,T}$, are thus interpolated from the F_N and F_T (determined using Equation (3) of the two adjacent disk elements at the same radius r (see Figure 1C). The various moments defined in Equations (5)–(8) and new global diagnostics (P and T) are then computed based on these "artificial blade forces." In the remainder of this paper, we will refer to this procedure as AD-B.

In this study, this methodology is applied in a post-processing step in order to follow exactly the VPM blade trajectories, including the initial transient due to the starting of the wind turbine. However, this procedure is also implemented to be performed online, during the simulation. It is relevant for large wind farm simulations, in order to avoid saving a large amount of AD data and post-processing calculations, but it is particularly important for load alleviation strategies, for example, applying an individual pitch control scheme within an AD framework[51] or future global wind farm control investigations.

10991824, 2022, 11, Downloaded from https://onlinelibrary.wiley.com/doi/10.1002/we.2772 by Bibliothecaire En Chef Uni Catholique De Louvain (Ucl), Wiley Online Library on [18/03/2024]. See the Terms and Conditions (https://onlinelibrary.wiley.com/terms-and-conditions) on Wiley Online Library for rules of use; OA articles are governed by the applicable Creative Commons License

In both codes, only the wind turbine blades are modeled; the tower and the hub are not represented. The VPM code does not capture the aeroelastic effects of the wind turbine blades, those thus act as rigid bodies. Although the fourth-order finite differences code has been extended and two-way coupled to an aeroelastic code,[52] this feature is currently only available for the AL method.

2.4 | Computation of the fatigue equivalent loads and damages

2.4.1 | Time domain

In this study, a fatigue analysis is first performed in the time domain, which is based on the rainflow counting (RFC) method[32] and a Palmgren–Miner rule[33] for linear fatigue damage accumulation. The RFC method uses the temporal signal of the loads and allows to count the number of cycles n_i for a particular load amplitude. The procedure for the damage estimate detailed in the following equations is based on the stress amplitude S_i; we will further adapt the methodology to the moment amplitude M_i. In this study, we assume that only the amplitude of a cycle contributes to the fatigue damage: the effect of the mean level of the cycle (through a Goodman correction,[53] for example) is here not added.

The cumulated damage, D, associated to the considered load time series can be calculated by applying a Miner's sum

$$D=\sum_{i=1}^{L_c}\frac{n_i}{N_i}, \tag{9}$$

where i and L_c represent the load case number and the total number of load cases, respectively; n_i is the number of cycles for the particular stress amplitude S_i; N_i is the number of S_i cycles that leads to failure. Using the S–N relation (also known as a Wöhler's curve) in the High-Cycle Fatigue zone for the considered material, the allowable number of cycles N_i of a stress amplitude S_i is given by

$$N_i=kS_i^{-m}, \tag{10}$$

where k and m are parameters dependent on the material. Equation (9) is thus re-expressed as

$$D=\sum_{i=1}^{L_c}\frac{n_i}{kS_i^{-m}}. \tag{11}$$

It is useful to express the fatigue damage in terms of an equivalent fatigue load, S_{eq}, which is the constant-amplitude loading that would, over an arbitrary number of cycles N_{eq}, cause an amount of damage equivalent to that of the original time series

$$D=\frac{N_{eq}}{kS_{eq}^{-m}}=\sum_{i=1}^{L_c}\frac{n_i}{kS_i^{-m}}\Leftrightarrow S_{eq}=\left(\sum_{i=1}^{L_c}\frac{n_iS_i^m}{N_{eq}}\right)^{\frac{1}{m}}. \tag{12}$$

In order to avoid introducing modeling errors in the computation of S_i from the available moment time series, the fatigue estimates are investigated in terms of equivalent moment values, M_{eq}. Assuming that the moment is proportional to the stress, M_{eq} is evaluated as

$$\mathrm{M}_{eq}=\left(\sum_{i=1}^{L_c}\frac{n_iM_i^m}{N_{eq}}\right)^{\frac{1}{m}}. \tag{13}$$

In the present study, M_i corresponds to a particular $M_{f,b}, M_{e,b}, M_y$, or M_t amplitude. The exponent m is here defined as 10 for M_f and M_e, which is a widely used value for blades made of fiberglass,[54] such as those of the NREL-5MW.[55] The yawing and tilting moments impact, among other components, the main shaft, which is usually made in forged steel[56]: m is chosen to be equal to 4, which is within the range between 3 and 5 typically used for the metallic wind turbine components.[57]

In the present study, we compare the different methods by considering ratios of M_{eq} or D:

$$\frac{M_{eq,1}}{M_{eq,2}}=\left(\frac{\sum_{i=1}^{L_{c,1}}n_{i,1}M_{i,1}^m}{\sum_{i=1}^{L_{c,2}}n_{i,2}M_{i,2}^m}\right)^{\frac{1}{m}}, \tag{14}$$

10991824, 2022, 11, Downloaded from https://onlinelibrary.wiley.com/doi/10.1002/we.2772 by Bibliothecaire En Chef Uni Catholique De Louvain (Ucl), Wiley Online Library on [18/03/2024]. See the Terms and Conditions (https://onlinelibrary.wiley.com/terms-and-conditions) on Wiley Online Library for rules of use; OA articles are governed by the applicable Creative Commons License

$$\frac{\frac{D_1}{D_2}=\sum_{i=1}^{L_{c,1}} n_{i,1}M_{i,1}^m}{\sum_{i=1}^{L_{c,2}} n_{i,2}M_{i,2}^m=\left(\frac{M_{eq,1}}{M_{eq,2}}\right)^m}, \tag{15}$$

with subscripts 1 and 2 being the considered methods (e.g., AD-B and VPM). This makes the results independent of N_{eq} or other material properties (except the m exponent).

2.4.2 | Frequency domain

Another type of approach estimates fatigue damage in the frequency domain,[38] by obtaining information equivalent to cycle counts directly from the one-sided PSD of the load fluctuations. We consider the Dirlik's (DK) method[39]: Although it was not originally designed for signals presenting a non-Gaussian distribution and with large periodic components, this counting procedure is often used in wind energy research and leads to the most accurate predictions.[36,41,42] In the present study, such an approach could allow to account for unresolved subgrid scales in the fatigue load estimation computed using the AD-B method at a coarse resolution, by using an extrapolated PSD. This will be detailed in Section 4.3. The DK procedure was developed by considering many different processes with power spectra of various shapes, computing their stress range distributions in the time domain via a RFC, and fitting a general expression for the stress range probability density function (pdf) in terms of *n*-th spectral moments, denoted m_n, and expressed as

$$m_n=\int_0 f^n PSD(f)df \tag{16}$$

with f is the frequency. The DK formula uses m_0, m_1, m_2, and m_4 (see below). The number of cycles n_{DK} for a given stress amplitude *S* is obtained with the expression

$$n_{DK}(S)=N_{DK}\ p_{DK}(S)dS\ . \tag{17}$$

N_{DK} is the total number of cycles during the considered time period and $p_{DK}(S)$ the pdf of the stress amplitude S. N_{DK} is estimated as the time period T_{DK} of the signal, multiplied by the expected number of peaks per second E[P],

$$N_{DK}=T_{DK}E[P]=T_{DK}\sqrt{\frac{m_4}{m_2}} \tag{18}$$

with E[P] that can be expressed in terms of m_2 and m_4. $p_{DK}(S)$ for the DK approach is a weighted combination of an exponential and two Rayleigh distributions:

$$p_{DK}(S)=\frac{1}{2\sqrt{m_0}}\left[\frac{G_1}{Q}e^{\left(-\frac{Z(S)}{Q}\right)}+\frac{G_2Z(S)}{R^2}e^{\left(-\frac{Z(S)^2}{2R^2}\right)}+G_3Z(S)e^{\left(\frac{-Z(S)^2}{2}\right)}\right], \tag{19}$$

with Z, the normalized stress range, and G_1, G_2, and G_3, the empirical distribution weight factors:

$$Z(S)=\frac{S}{2\sqrt{m_0}},\quad G_1=\frac{2\left(x_m-\alpha_2^2\right)}{1+\alpha_2^2},\quad G_2=\frac{1-\alpha_2-G_1+G_1^2}{1-R},\quad G_3=1-G_1-G_2\,, \tag{20}$$

and Q and R defined as

$$Q=\frac{1.25(\alpha_2-G_3-G_2R)}{G_1},\quad R=\frac{\alpha_2-x_m-G_1^2}{1-\alpha_2-G_1+G_1^2}. \tag{21}$$

α_2 is a regularity factor representing the expected ratio of zero-crossings to peaks and x_m, a mean frequency,

10991824, 2022, 11, Downloaded from https://onlinelibrary.wiley.com/doi/10.1002/we.2772 by Bibliothecaire En Chef Uni Catholique De Louvain (Ucl), Wiley Online Library on [18/03/2024]. See the Terms and Conditions (https://onlinelibrary.wiley.com/terms-and-conditions) on Wiley Online Library for rules of use; OA articles are governed by the applicable Creative Commons License

$$\alpha_2 = \frac{m_2}{\sqrt{m_0 m_4}}\,, \quad x_m = \frac{m_1}{m_0}\sqrt{\frac{m_2}{m_4}}\,. \tag{22}$$

In a discrete form and expressed in terms of moment, Equation (17) becomes

$$n_{DK,i} = N_{DK}\, p_{DK,i} \Delta M\,. \tag{23}$$

$p_{DK,i}$ is thus the pdf of a given moment amplitude M_i, and Equation (16) implies the PSD of the moment fluctuations. The cumulated damage D_{DK} and the equivalent fatigue load $M_{eq,DK}$ are then computed in a similar way as those of Equations (13)–(15). In order to compare the DK predictions to the RFC results, it is interesting to superpose the number of cycles per load amplitude computed with the two approaches. For the RFC method, the total range of the moment amplitudes is divided into a certain number of bins of width ΔM: The same moment amplitude discretization is thus used for computing $n_{DK,i}$ (the width and the number of bins varying according to the considered moment and the flow case).

3 | CONFIGURATION

In this study, we aim at assessing the fatigue loads estimated using the AD-B approach for an isolated wind turbine, by comparing them to those obtained using the VPM method at a finer resolution. We here consider the "NREL offshore 5-MW baseline wind turbine"[55] (here denoted NREL-5MW), at three particular operating conditions: just after the start-up of the rotor ($\overline{U} = 5$ m/s and a tip-speed ratio, λ, equal to 10.24), during the optimum operating condition ($\overline{U} = 9$ m/s and $\lambda = 7.55$) and during the rated operation ($\overline{U} = 14$ m/s and $\lambda = 5.7$). $\overline{U}$ represents the time-averaged inflow velocity, and λ is computed with that wind speed, that is, $\lambda = \Omega R_{tip}/\overline{U}$ (R_{tip} is equal to 63 m for the NREL-5MW[55]). The main parameters of these operating conditions are reported in Table 1. The controller is inactive to avoid introducing discrepancies between the AD-B and the VPM methods due to a different rotor response to the control scheme. Consequently, the blade pitch angle and the rotor speed are maintained constant during the whole simulation time. The wind turbine operates in a turbulent wind with a turbulence intensity of about 7%; the generation of the turbulence is detailed below. For the AD-B procedure, we reproduce the blade trajectories recovered from the VPM approach.

In this paper, we focus our analysis on a turbine impacted by incoming turbulent fluctuations. This will allow us to investigate the impacts of the wind turbine model and the resolution on a wide range of load cycle amplitudes. Considering more fundamental cases, such as laminar shear inflows or a wind turbine in a yawed configuration without incoming inflow turbulence, would result in fatigue load fluctuations at one frequency only and restrict the analysis.

The domain size, the resolution, and the location of the wind turbine in each code are reported in Table 2. As the VPM method handles exactly the unbounded transverse directions using a compact mesh solely containing the vorticity, the width of the mesh can be small. The domain size of the VPM method corresponds to the initial one as the domain is adapted over the course of the simulations to encompass all the vorticity. The resolution is also very fine (128 points per D, where $D = 2R_{tip}$, the NREL-5MW diameter). The simulation domain for the AD method is larger to limit the effect of the boundaries on the resulting loads and to have a fair comparison with the VPM approach. The resolution is chosen to be close to that used in wind farm simulations (16 points per D), as this AD approach aims to be used in those applications.

TABLE 1 NREL-5MW: Operating points

$\overline{U}$ (m/s)	λ	Ω (RPM)	γ (°)
14	5.7	12.10	8.7
9	7.55	10.30	0
5	10.24	7.8	0

TABLE 2 Domain size, resolution, and wind turbine position for the AD and the VPM approaches

	AD	VPM
$L_x \times L_y \times L_z$	$8D \times 9D \times 9D$	$8D \times 3D \times 3D$
$N_x \times N_y \times N_z$	$128 \times 144 \times 144$	$1024 \times 384 \times 384$
WT position	(3D, 4.5D, 4.5D)	(3D, 1.5D, 1.5D)

10991824, 2022, 11, Downloaded from https://onlinelibrary.wiley.com/doi/10.1002/we.2772 by Bibliothecaire En Chef Uni Catholique De Louvain (Ucl), Wiley Online Library on [18/03/2024]. See the Terms and Conditions (https://onlinelibrary.wiley.com/terms-and-conditions) on Wiley Online Library for rules of use; OA articles are governed by the applicable Creative Commons License

Both VPM and AD methods currently do not include dynamic stall effects. The present wind conditions and turbine operating points will lead to a flow that will remain attached to the blade most of the time, and if dynamic effects occur, they will be located in the inboard part of the blade (not shown here), for which the contribution to the total moment is limited, due to the presence of the local radius in the moment computation. The use of static polar data only is thus an acceptable simplification in this study. However, the dynamic stall effects are no more negligible if we consider strong shear, important variations in the incoming velocity (due to a gust or the presence of an upstream wake) or a wind turbine operating with a yaw offset, as it was highlighted in several research works.[13,58] As the AD method will be used in investigations about global control strategies, which will place more wind turbines under yawed and partially waked inflow conditions, it is thus relevant to add dynamic stall effects in future simulations. Typical dynamic stall models used in wind energy applications,[25,59] based on the Leishman–Beddoes (LB) model,[60] could be included. The implementation of the LB model is possible for an AD method, although it requires some modifications and additional iterations.

3.1 | Generation of the inflow turbulent fluctuations

The turbulence field is generated using the Mann algorithm[61] and is added to the mean inflow velocity. A turbulence intensity of about 7% is considered for the three operating conditions, which is typical of the offshore environment. In order to compare the unsteady loads, it is important that the same turbulent structures impact the wind turbine at the same times in the two simulations. Only one synthetic turbulence box for the AD-B and the VPM methods is thus generated, and the resolution of the resulting turbulence field is adapted according to the method. The main parameters of the box for each wind speed are reported in Table 3. As the initial turbulence box is smaller than the AD simulation domain, the turbulent field is only added on a square of $3D \times 3D$ at the inflow, centered around the wind turbine position.

For each wind speed, three boxes are generated, each one having a particular seed for the random number generator in the Mann algorithm, and the statistics are computed over the three turbulence seeds. This aims at having a better representation of the rarest events, which may significantly contribute to the fatigue damages.[35]

4 | RESULTS

4.1 | Comparison of power and thrust

Before analyzing the fatigue loads, we compare in Figure 2 the power and thrust histories given by the two codes for the three operating conditions and one particular Mann turbulence box. The results for the simulations with the two other Mann turbulence boxes are similar, and the following discussion is thus valid for the three sets of turbulence fields. We here want to verify if the wind turbine is impacted by the same structures in the two codes and to compare the global statistics obtained with the two approaches. Additionally, we compare the initial AD power and thrust with those computed based on the re-interpolated three blade forces, that is, the AD-B approach.

In order to have a clearer comparison in Figure 2, the power and thrust histories of the VPM results are filtered using a moving average that attenuates the oscillations due to the blades rotation. The results for the AD-B approach are not filtered, to highlight the differences with the initial AD power and thrust. We only show the results for a time window corresponding to the Mann period ($T_{Mann} = 32D/\overline{U}$). A last general remark concerns the power for the lowest λ: as the controller is inactive, the power signal can, at times, widely exceed the 5.3 MW of mechanical power of the reference machine.[55]

We first compare the AD results to those obtained using the VPM method. For the lowest λ, the power and thrust histories are very similar for both codes. However, there are some time periods where the discrepancies are slightly higher, that is, around $t^* = 15$ or between $t^* = 30$ and 35, with $t^* = t\overline{U}/D$. They correspond to time periods where the flow structures slightly diverge between the two codes (it is probably due to differences in resolutions, codes and treatment of the turbulence). That is highlighted in Figure 3, where we compare the disk-averaged velocity

TABLE 3 Turbulence box: roughness length (y_0), turbulence intensity (TI), and Mann period (T_{Mann}) for each wind speed

$\overline{U}$ (m/s)	y_0 (mm)	TI (%)	$T_{Mann} = L_{x,Mann}/\overline{U}$ (s)
14	2.75	≃7 %	288
9	3.86	≃7 %	448
5	8.25	≃7 %	806.4

Note: The box size is the same for all the wind speeds, with $L_{x,Mann} \times L_{y,Mann} \times L_{z,Mann} = 32D \times 3D \times 3D$. The turbulence field is generated for the NREL-5MW hub height (90 m) and fitted to the three components of the Kaimal spectrum.[61]

10991824, 2022, 11, Downloaded from https://onlinelibrary.wiley.com/doi/10.1002/we.2772 by Bibliothecaire En Chef Uni Catholique De Louvain (Ucl), Wiley Online Library on [18/03/2024]. See the Terms and Conditions (https://onlinelibrary.wiley.com/terms-and-conditions) on Wiley Online Library for rules of use; OA articles are governed by the applicable Creative Commons License

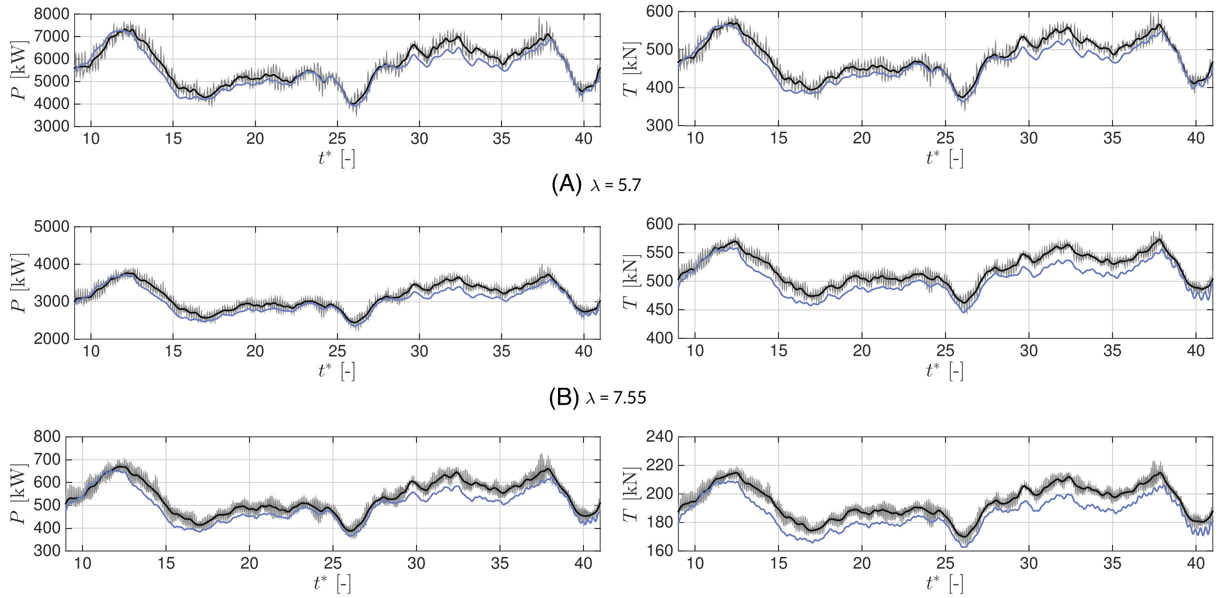

FIGURE 2 Mechanical power and thrust (P and T) for VPM (thick blue solid line), AD (thick black solid line), and AD-B (thin gray solid line) methods. The results are shown for the three tip-speed ratios

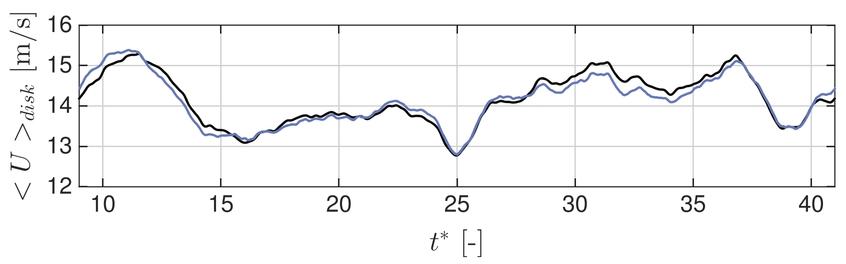

FIGURE 3 Disk-averaged axial velocity for simulations without wind turbine for $\overline{U} = 14$ m/s in the VPM code (blue solid line) and in the FD4 code (blue solid line). The diameter of the disk corresponds to that of the NREL-5MW

TABLE 4 Time-averaged power and thrust for the VPM simulations and percentage difference between the disk approaches (AD and AD-B) and the VPM method

case	Power (kW)	Power difference (%)		Thrust (kN)	Thrust difference (%)	
λ	VPM	AD	AD-B	VPM	AD	AD-B
5.7	5496.74	3.60	3.60	464.43	3.30	3.30
7.55	3007.61	4.14	4.14	504.22	3.33	3.33
10.24	502.00	6.55	6.55	185.94	4.42	4.42

at the rotor position for a flow without wind turbine in the two codes, for one particular turbulence box and $\overline{U} = 14$ m/s. The same behavior is observed for the two other wind speeds (not shown here).

We also observe that the discrepancies between the AD and the VPM results increase when λ increases. In addition to inflow variations discussed above, the larger errors observed at this particular λ are probably due to the loading distribution on the blade, which is high near the blade tip[30]: The AD method misses the decrease in F_N and F_θ, even when it is supplemented with the tip-loss correction, due to its coarser resolution. Conversely, for the lowest λ, the blade loading is concentrated on the inboard part,[30] and the impact of the coarse resolution of the AD method is less marked. This is translated in the power and thrust averaged values, reported in Table 4. We show the percentage difference between the VPM and the AD results in terms of power and thrust averaged over one T_{Mann} period ($\overline{P}$ and $\overline{T}$, respectively). We consider that the VPM approach produces our reference results, and we use the unfiltered VPM data for the averages. The largest differences are observed for the highest λ,

10991824, 2022, 11, Downloaded from https://onlinelibrary.wiley.com/doi/10.1002/we.2772 by Bibliothecaire En Chef Uni Catholique De Louvain (Ucl), Wiley Online Library on [18/03/2024]. See the Terms and Conditions (https://onlinelibrary.wiley.com/terms-and-conditions) on Wiley Online Library for rules of use; OA articles are governed by the applicable Creative Commons License

where the AD method overestimates $\overline{P}$ and $\overline{T}$ by 6.5% and 4.5%, respectively. For moderate and low λ, the discrepancies between the two approaches remain lower than 4.2% and 3.3% for $\overline{P}$ and $\overline{T}$, respectively.

Additionally, we see in Figure 2 that the power and thrust computed with the AD-B method are very close to the initial AD power and thrust, and this for all operating conditions. This is confirmed by the time-averaged results presented in Table 4. The percentage difference with the VPM results remains the same for the AD and the AD-B methods; $\overline{P}$ and $\overline{T}$ recovered by the re-interpolated blades are thus nearly equal to those obtained with the initial AD method.

4.2 | Moment densities

Before performing a fatigue analysis in terms of M_{eq} and D, we first compare the fatigue loads as pdfs and one-sided PSDs. This will highlight some behaviors that could explain the differences/similarities obtained in terms of fatigue estimates. All the statistics are computed over one period T_{Mann} and over the three turbulence seeds. Moreover, for the root bending moments, the statistics are accumulated over the three blades: In the remainder of the paper, the notation M_f and M_e will be thus used for the flapwise and the edgewise moments, respectively.

In Figure 4, the pdf of the moments is shown for the three λ. The AD-B approach leads to results very similar to the VPM approach for all the moments and the operating conditions. However, we notice that it has mean root bending moments that are slightly higher, especially for

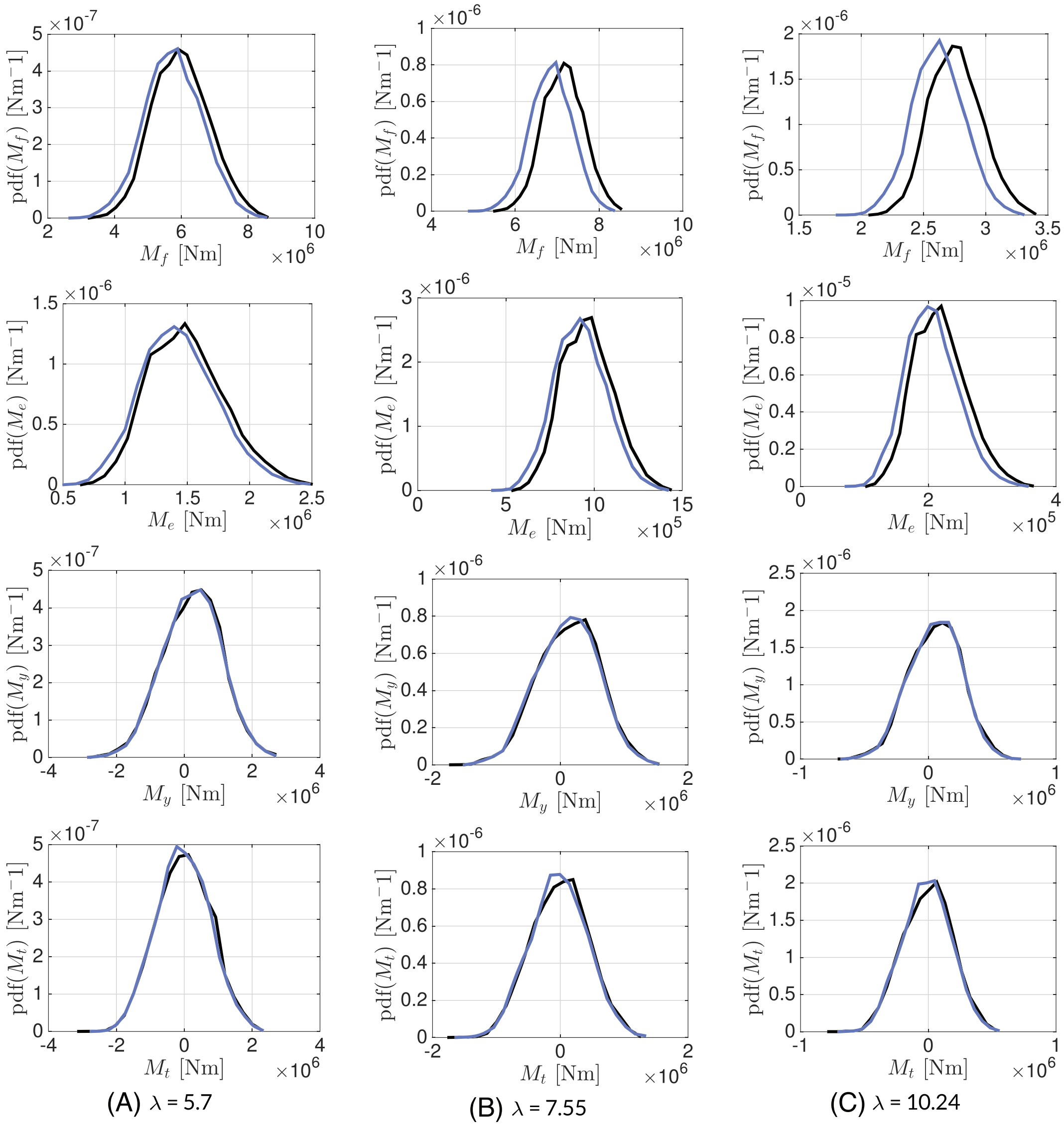

FIGURE 4 PDFs of M_f, M_e, M_y, and M_t (AD-B (black solid line) and VPM (blue solid line). The results are shown for the three λ

10991824, 2022, 11, Downloaded from https://onlinelibrary.wiley.com/doi/10.1002/we.2772 by Bibliothecaire En Chef Uni Catholique De Louvain (Ucl), Wiley Online Library on [18/03/2024]. See the Terms and Conditions (https://onlinelibrary.wiley.com/terms-and-conditions) on Wiley Online Library for rules of use; OA articles are governed by the applicable Creative Commons License

10991824, 2022, 11, Downloaded from https://onlinelibrary.wiley.com/doi/10.1002/we.2772 by Bibliothecaire En Chef Uni Catholique De Louvain (Ucl), Wiley Online Library on [18/03/2024]. See the Terms and Conditions (https://onlinelibrary.wiley.com/terms-and-conditions) on Wiley Online Library for rules of use; OA articles are governed by the applicable Creative Commons License

moderate and high λ: It is consistent with the already observed AD-B power and thrust that exhibit an offset with those obtained with the VPM method. At each λ and for each type of moment, the width of the pdfs is similar for the AD-B and the VPM methods: This highlights that the two wind turbine models globally capture the same moment fluctuations.

With an AD approach at coarser resolutions, we cannot expect to capture the load fluctuations at frequencies as high as those captured by the high resolution VPM simulations. This is highlighted with the PSD of the moment fluctuations (see Figure 5). The spectra for the VPM and the AD-B loads can be seen to agree very well over a broad band at low frequencies, but the moments obtained with the AD-B method and its "virtual" blades drop beyond a certain cut-off frequency f_c. f_c, normalized by the rotational frequency f_Ω, is between 10 and 15. This f_c is smaller than the cut-off frequency related to the time step of the AD simulations. This is explained by the Courant–Friedrichs–Lewy (CFL) number that cannot exceed 0.2–0.25 in the FD4 code, in order to avoid numerical oscillations. In the present simulations, the CFL varies from 0.1 ($\lambda = 5.7$) to 0.13 ($\lambda = 10.24$): Consequently, the temporal resolution is very fine compared to the mesh resolution, and the energy content is thus slightly degraded in the high frequencies, as it is not well captured by the mesh.

Globally, the good agreement over low frequencies hints at a potential extrapolation of the AD-B spectral behavior to high frequencies: This will be discussed in details in the next section (Section 4.3). However, in terms of yaw and tilt moments at $\lambda = 7.55$ and 10.24, we observe more

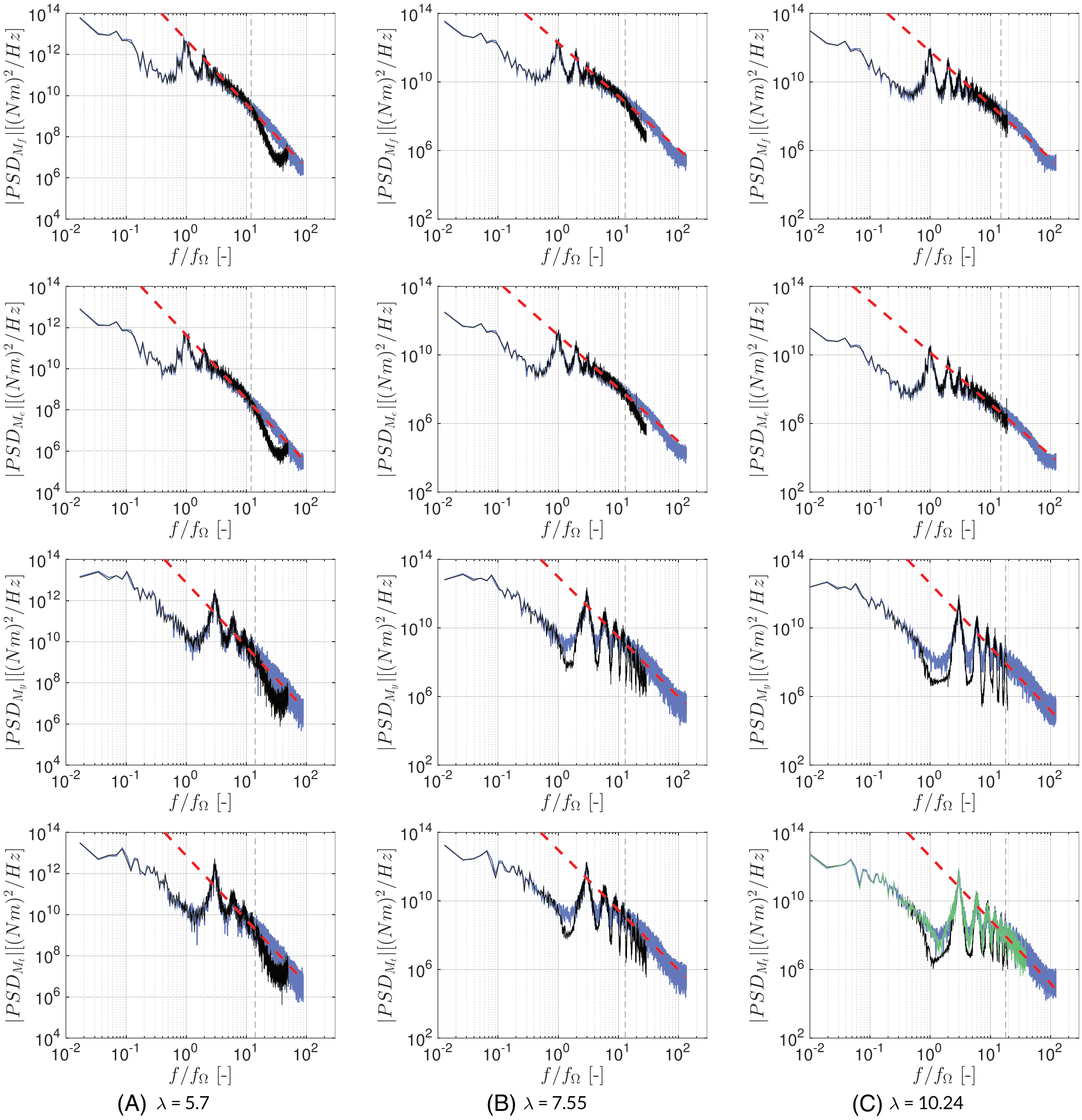

FIGURE 5 PSDs of M_f, M_e, M_y, and Mt (AD-B (black solid line) and VPM (blue solid line). The results are shown for the three λ. The green solid line shows the results for the AD-B approach with a resolution twice finer as the initial one. The red dashed line corresponds to the extrapolated PSDs for the AD-B approach. The vertical gray dashed line corresponds to the cut-off frequency from which the extrapolated curves are used in the DK_{ext} method (see Section 4.3)

discrepancies: The AD-B approach presents lower PSD values in the valleys, while it captures the peaks very well. A potential explanation is related to λ. At high λ, the loads are more greatly influenced by the rotor rotation, making the signals more periodic: This effect is reinforced for the AD-B approach at a coarse resolution, as the model only captures the large structures, and the reconstructed signal could thus present more harmonics and less other frequencies. This effect may be reinforced for M_y and M_t, as they are already filtered quantities. If we perform AD simulations with a resolution that is twice as fine as the initial one, we see that this particular behavior is mitigated, with a PSD that becomes closer to that obtained with the VPM approach (see an example for M_t at $\lambda = 10.24$ in Figure 5C, the tendency is similar for M_y and for $\lambda = 7.55$). The discrepancies thus appear to be related to the difference of resolution, rather than linked to a difference of wind turbine model.

4.3 | Fatigue equivalent loads

4.3.1 | Comparison of the number of cycles per load amplitude

We first compare the number of cycles per load amplitude, n_i and $n_{DK,i}$, obtained using the RFC and the DK methods, respectively. The results are reported in Figure 6. For each λ, the results are accumulated over the three turbulence boxes: The RFC is thus applied on each turbulent simulation, and n_i is accumulated over the three simulations. The number of cycles is moreover accumulated over the three blades for M_f and M_e. For the DK method, the PSDs presented in Section 4.2 are used for computing the spectral moments of Equation (16). The period T_{DK} of Equation (18) corresponds to $3T_{Mann}$ for M_y and M_t and to $6T_{Mann}$ for M_f and M_e (as the three blades are taken into account).

The discussion is structured into three main points. First, n_i obtained using the RFC approach is analyzed. Second, the number of cycles obtained using the DK counting method is discussed, in light of the RFC results. Finally, a simple modification is proposed in the DK procedure for the AD-B approach, in order to decrease several discrepancies observed between the AD-B and the VPM methods.

4.3.2 | RFC approach

Globally, we see that the distribution of n_i is similar in both codes, even if we observe several discrepancies. As excepted, for all the λs and types of moment, the AD-B procedure presents lower n_i at the small moment amplitudes, due to its coarse resolution. However, we will see that these "relatively" large differences do not strongly impact the fatigue damage estimate. It is partly due to the presence of the m-exponent (up to a value of 10 in our study) that reinforces the contribution of the large moment amplitudes to M_{eq} and especially to D.

Regarding these cycles of large amplitude, their distribution is marginally captured by the simulations as their number can be just one or even an half. This corresponds to the rarest events occurring in the flow simulations. As the contribution of those cycles is significant on M_{eq} and D, if n_i is equal to 1 for the VPM method but 0 for the AD-B method, this could increase the discrepancies between the fatigue estimates. In order to "fill" those scales and having n_i considerably higher than one, more simulations with different turbulence realizations and a same TI should be performed or T_{Mann} should be increased. This could potentially lead to the apparition of new very large but not yet observed cycles, mitigating the beneficial effect of the proposed solutions, but the use of the Mann algorithm should normally limit this risk. However, this would considerably increase the computational costs, mainly for the VPM method.

DK approach

By comparing the RFC results to those obtained using the DK method in each code, we see that this last counting procedure presents a "smoother" distribution and fills the cycles of all the large moment amplitudes. In fact, if short time series are used to extrapolate fatigue damage for longer operational periods (as is common practice in wind turbine engineering[35]), the DK method could provide a better estimation than the RFC approach, as it was already noticed in the literature.[36,41]

However, for moments of middle amplitude, the DK method leads to predictions that underestimate n_i. This is due to the marked periodicity of the considered moment signals (well noticeable in the PSDs of Figure 5), which is not well captured by the DK approach. Moreover, some effects that could reinforce the periodic components of the signal and increase the discrepancies between the two counting methods are omitted in the present study. In particular, we mention the wind shear and the gravitational loads that tend to move the periodicity peak in larger moment amplitudes for M_e.[35] Nevertheless, it appears that the DK method was considered in several research studies of wind turbine fatigue estimates, which accounted of all those effects, and that it led to acceptable resulting damage predictions.[34,36]

For moments of small amplitudes, the DK approach overestimates n_i. For the VPM method, this is particularly marked for the two or three smallest moment amplitudes, while it is slightly shifted in larger amplitudes for the AD-B approach. The divergence between the AD-B and the VPM methods is due to the PSD cut-off at high frequencies for the AD-B model. On the contrary, for moments of middle and large amplitudes, we see that $n_{DK,i}$ is very similar for the VPM and the AD-B methods.

10991824, 2022, 11, Downloaded from https://onlinelibrary.wiley.com/doi/10.1002/we.2772 by Bibliothecaire En Chef Uni Catholique De Louvain (Ucl), Wiley Online Library on [18/03/2024]. See the Terms and Conditions (https://onlinelibrary.wiley.com/terms-and-conditions) on Wiley Online Library for rules of use; OA articles are governed by the applicable Creative Commons License

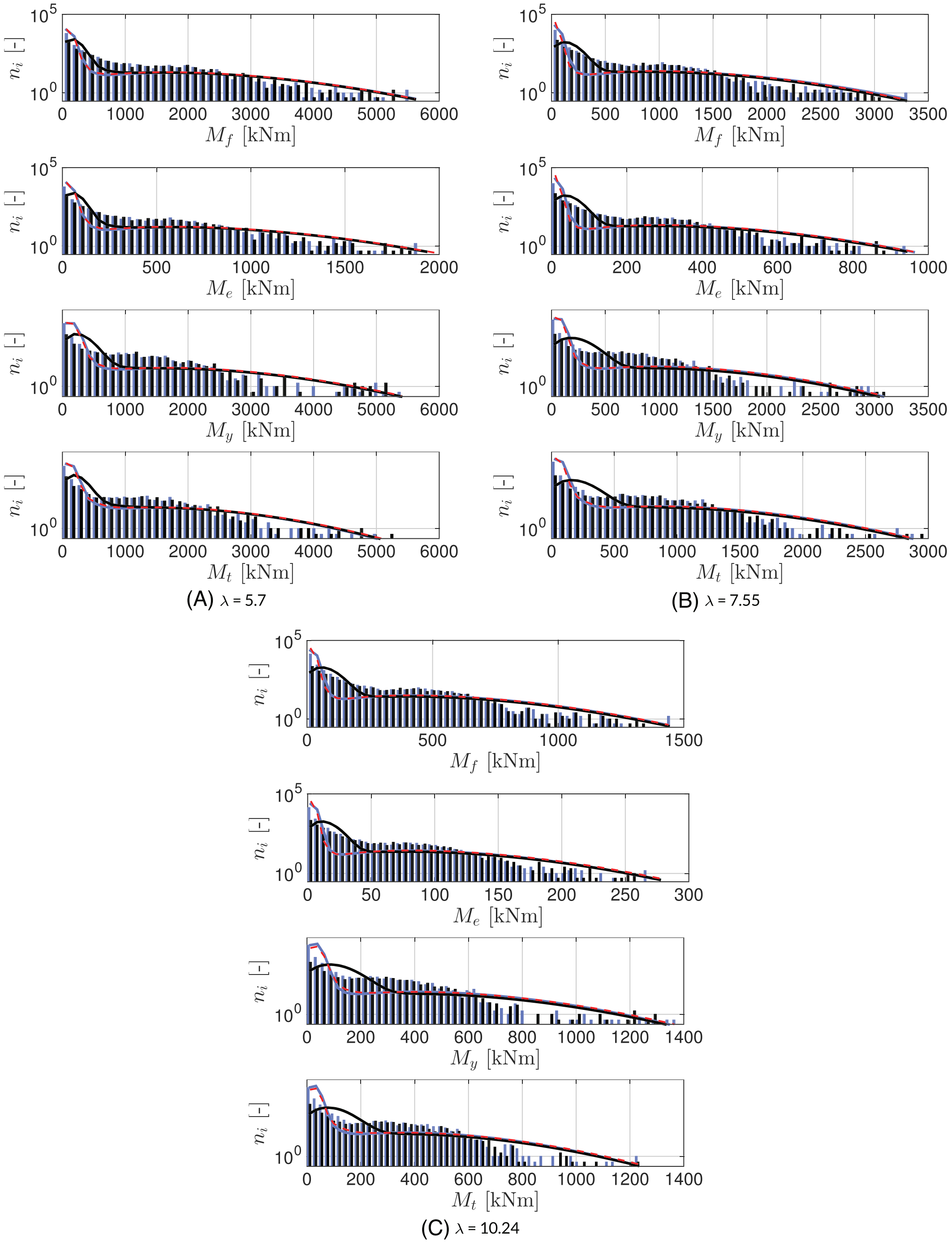

FIGURE 6 Number of cycles for M_f, M_e, M_y, and M_t, for the AD-B (black bars and lines) and the VPM (blue bars and lines) approaches. The results are shown for the three λ. The bars of the histogram are obtained using the RFC approach, while the distribution reported with the solid lines are computed using the DK method. The red dashed line corresponds to the distribution computed using the DK_{ext} procedure for the AD-B approach

DK_{ext} approach

Let us now attempt to reduce the discrepancies between the two approaches, by extrapolating the PSDs obtained using the AD-B method. We extend the curves with a power law $C_{M_i}(f/f_\Omega)^{-\beta_i}$: C_{M_i} and β_i are determined in order to fit to the PSD before its drop, where the curve is nearly a straight line in a log-log scale. The parameters are adapted for each λ and for each type of moment. As highlighted in Section 4.2, the extrapolation is more challenging for M_y and M_t, mainly for the two highest λ. An ideal situation would be to conserve the same exponent β_i for all the moments, but β_i varies a lot, and it is very complex to extract only one value that fits well all the PSD curves. In a first approach, we thus compute our parameters for M_y and M_t in order to follow the behavior of the VPM method in the highest frequencies. We report the extrapolations on the

10991824, 2022, 11, Downloaded from https://onlinelibrary.wiley.com/doi/10.1002/we.2772 by Bibliothecaire En Chef Uni Catholique De Louvain (Ucl), Wiley Online Library on [18/03/2024]. See the Terms and Conditions (https://onlinelibrary.wiley.com/terms-and-conditions) on Wiley Online Library for rules of use; OA articles are governed by the applicable Creative Commons License

PSD curves in Figure 5. The extrapolated curves are used from a certain f/f_{Ω}, different according the moment and the operating condition (see Figure 5). This particular frequency is determined as the one from which the PSD of the AD-B method begins to drop. For frequencies lower than this particular value, the initial AD-B curves are conserved, as they are already close to those of the VPM method.

The cycle distributions computed using these extrapolated PSDs are reported on Figure 6; This method will be denoted DK_{ext} in the remainder of this paper. Globally, the use of the DK_{ext} procedure for the AD-B approach leads to a cycle distribution at the smallest moment amplitudes similar to that obtained using the VPM method. However, the DK_{ext} procedure may also slightly change $n_{DK,i}$ at larger moment amplitudes: This could mitigate or even annihilate the beneficial effect of a better cycle distribution at the small moment amplitudes.

Comparison of the equivalent fatigue loads and fatigue damages

We first compare the two counting methods; we report in Table 5 the fatigue estimates by computing the ratios $M_{eq,DK}/M_{eq,RFC}$ and D_{DK}/D_{RFC}. We also report the ratios $M_{eq,DK_{ext}}/M_{eq,RFC}$ and $D_{DK_{ext}}/D_{RFC}$ for the AD-B approach. Globally, the DK method leads to M_{eq} and D higher than those computed using the RFC procedure, which is a common ascertainment in literature.[36] This is mainly due to the differences observed in the n_i distribution at large moment amplitudes. In Burton et al,[34] it is mentioned that the ratio between the DK and the RFC results can reach 2.4 for the damages, which corresponds to the order of magnitude of the ratios presented in Table. 5. We notice a slightly better agreement between the two methods when λ decreases. Indeed, loads for a low λ display a noisier and less periodic behavior, while the loads for a higher λ are more influenced by the periodicity of the rotor rotation (noticeable in Figures 5 and 6. We thus expect to observe poorer performances at high λ.

It is not trivial to draw conclusions from these results and to highlight the most suitable approach for computing the fatigue damages. The RFC procedure is normally more accurate, as it really counts the number of loading cycles. However, a fatigue study usually aims at estimating the damages on a period covering the whole life time of the wind turbine. It is simply not possible to obtain sufficiently long temporal signals with numerical studies such as the present ones or these used to predict rotor loads for a potential site installation. Usually, an analytical distribution is fitted to the shot-term RFC data or a statistical extrapolation of the uppertail of stress ranges is employed,[35] in order to predict the number of cycles of very large but not yet observed stress amplitudes expected over the whole rotor life. Ragan and Manuel[36] used an extrapolation technique[62] for adjusting the RFC method and showed that the discrepancies between the RFC and the DK methods were reduced. However, determining what is the best method for estimating fatigue life or extrapolating the RFC method is not the main subject of this paper, and we leave this for further investigations.

When we compare the DK_{ext} and the RFC methods for the AD-B procedure, we see that the discrepancies are higher than those observed between the DK and the RFC approaches. This will be discussed at the end of the present section.

In Table 6, for each counting procedure, we show the ratios of the AD-B fatigue estimates over those obtained using the VPM method. We first discuss the RFC results. Globally, for M_{eq}, the results are very close to each other, with less than 3.5% of differences. The differences observed in terms of n_i for the small moment amplitudes in Figure 6 do not strongly impact the resulting fatigue estimates, and the AD-B approach at a coarse resolution captures wind events that significantly impacts the fatigue damage. For D, the discrepancies can be higher, which is due to the m-exponent of Equation (15): As m is equal to 10 for M_f, the 3.3% of differences observed in M_{eq} at $\lambda = 10.24$ become nearly 30% in D.

For the DK method, M_{eq} obtained from the VPM and the AD-B results are also close to each other, with a 4% maximum difference for M_y at $\lambda = 10.24$. The impact of this difference on D is quite small (slightly more that 15%) because $m = 4$ for M_y. On the contrary, for M_f and $\lambda = 7.55$, as $m = 10$, the 2% of differences observed for M_{eq} become 18.3% for D.

TABLE 5 Ratios between the DK and the RFC approaches for M_{eq} and D, computed based on the AD-B and VPM results. AD-$B_{DK_{ext}}$ denotes here the AD-B equivalent moments and damages computed using the DK_{ext} method

Case Code		$\lambda = 5.7$			$\lambda = 7.55$			$\lambda = 10.24$		
		AD-B	AD-$B_{DK_{ext}}$	VPM	AD-B	AD-$B_{DK_{ext}}$	VPM	AD-B	AD-$B_{DK_{ext}}$	VPM
$M_{eq,DK}/M_{eq,RFC}$	M_f	1.080	1.089	1.067	1.089	1.106	1.078	1.115	1.135	1.090
	M_e	1.076	1.093	1.080	1.095	1.121	1.101	1.116	1.144	1.112
	M_y	1.091	1.116	1.100	1.104	1.165	1.138	1.135	1.202	1.158
	M_t	1.108	1.126	1.115	1.121	1.168	1.129	1.143	1.194	1.136
D_{DK}/D_{RFC}	M_f	2.167	2.335	1.921	2.344	2.732	2.127	2.957	3.550	2.376
	M_e	2.084	2.441	2.157	2.474	3.132	2.10	2.983	3.830	2.895
	M_y	1.414	1.553	1.465	1.487	1.840	1.674	1.658	2.084	1.795
	M_t	1.505	1.609	1.548	1.580	1.861	1.622	1.706	2.033	1.663

10991824, 2022, 11, Downloaded from https://onlinelibrary.wiley.com/doi/10.1002/we.2772 by Bibliothecaire En Chef Uni Catholique De Louvain (Ucl), Wiley Online Library on [18/03/2024]. See the Terms and Conditions (https://onlinelibrary.wiley.com/terms-and-conditions) on Wiley Online Library for rules of use; OA articles are governed by the applicable Creative Commons License

TABLE 6 Ratios between the AD-B and the VPM methods for M_{eq} and D computed based on the RFC and the DK procedures. The notation DK_{ext} corresponds the DK fatigue estimates obtained using the extrapolated PSDs for the AD-B approach

Case		$\lambda = 5.7$			$\lambda = 7.55$			$\lambda = 10.24$		
Counting method		RFC	DK	DK_{ext}	RFC	DK	DK_{ext}	RFC	DK	DK_{ext}
$M_{eq,AD\text{-}B}/M_{eq,VPM}$	M_f	0.983	0.995	1.002	0.971	0.980	0.995	0.967	0.988	1.006
	M_e	1.004	1.001	1.017	0.987	0.982	1.005	1.002	1.006	1.031
	M_y	1.008	0.999	1.023	0.993	0.964	1.017	0.979	0.960	1.017
	M_t	1.016	1.009	1.026	0.978	0.972	1.012	0.969	0.975	1.019
$D_{AD\text{-}B}/D_{VPM}$	M_f	0.840	0.874	1.022	0.742	0.817	0.953	0.711	0.885	1.063
	M_e	1.042	1.006	1.179	0.876	0.830	1.051	1.025	1.056	1.355
	M_y	1.034	0.998	1.096	0.973	0.864	1.069	0.920	0.850	1.068
	M_t	1.067	1.037	1.110	0.915	0.891	1.050	0.881	0.904	1.077

For moderate and high λ, the use of the DK_{ext} procedure for the AD-B approach globally helps to decrease the discrepancies with the VPM method. In fact, the use of extrapolated PSDs changes $n_{DK,i}$ in the whole range of moment amplitudes, because the spectral moments of Equation (16) are different from those computed using the initial PSDs. This is the change in the middle and large moment amplitudes that finally reduces or increases the discrepancies between the AD-B and the VPM results. This also explains the increase of differences between the ratios DK/RFC and DK_{ext}/RFC for the AD-B approach in Table 5.

Figure 7 highlights this behavior, where $n_i M_i^m$ is reported as a function of M_i in order to emphasize the contribution of each loading cycle in the fatigue estimates. For the sake of clarity, we only show the results for $\lambda = 5.7$ and 7.55; the discussion for $\lambda = 7.55$ remains valid for $\lambda = 10.24$. Globally, we see that the smallest amplitudes are totally negligible (it was highlighted in Veers[35]). For $\lambda = 7.55$ and M_y and M_t, the DK_{ext} procedure clearly helps to the make the AD-B curve closer to the VPM one at the moment amplitudes that contribute the most to M_{eq} and D. The same remark can be made for M_f and M_e, but, as $m = 10$, these are the largest moment amplitudes that contribute the most to the fatigue damage. For the lowest λ, on the contrary, the DK_{ext} procedure increases the differences between the AD-B and the VPM methods, because it slightly changes a n_i distribution that was initially very close to the VPM one (see Figure 7A). For that operating condition, the DK_{ext} procedure only appears useful for M_f.

This study tends to demonstrate that the use of the DK_{ext} procedure can, at some operating conditions, improve the full fatigue picture provided by the AD-B method. However, the DK_{ext} method is very sensitive to the extrapolation parameters, which are not always trivial to determine from the initial PSDs. Moreover, Figure 7 clearly shows that the cycle distribution and the final contribution of each moment amplitude is quite different between the time domain and the spectral counting methods. It would be thus interesting to further investigate the proposed PSD extrapolation, in combination to an innovative spectral counting method that brings to a n_i distribution typical of that observed for wind turbine components.

4.4 | Impact of the resolution

Our simulations consider a grid resolution of 16 points per diameter, as it is a good compromise between accuracy and efficiency for both wind turbine and wake behaviors at a wind farm scale. We assume that the accuracy of the fatigue estimates would decrease if we coarsen the grid to eight points per D. However, as load cycles of medium and large amplitudes contribute the most to the fatigue damages, which may be expected to be still captured by a disk at a coarser resolution, the decrease in accuracy might be not so important. It could be interesting to perform simulations with eight points per D in order to quantify the actual impacts for the blade and rotor loads. A coarser resolution also impacts the numerical and the subgrid scale dissipations. One can thus expect such a coarse grid to produce a different wake behavior, in terms of wake meandering, velocity recovery, or level of turbulence. As the AD method will be deployed in wind farm simulations, it is important that the wake phenomena are still accurately captured. The use of a grid resolution of eight points per D should be thus also verified in terms of wake statistics.

Increasing the resolution should normally improve the results and decrease the discrepancies between the AD-B and the VPM results. Results reported on Figure 5C for the AD-B simulation performed on a grid that is twice finer tend to confirm this assumption. However, as highlighted in the paper and recalled above, the AD-B at a resolution of 16 points per D captures well the cycles of medium and large amplitudes. The improvement in accuracy with simulations in finer grids might be moderate. Again, this should be verified by additional simulations.

10991824, 2022, 11, Downloaded from https://onlinelibrary.wiley.com/doi/10.1002/we.2772 by Bibliothecaire En Chef Uni Catholique De Louvain (Ucl), Wiley Online Library on [18/03/2024]. See the Terms and Conditions (https://onlinelibrary.wiley.com/terms-and-conditions) on Wiley Online Library for rules of use; OA articles are governed by the applicable Creative Commons License

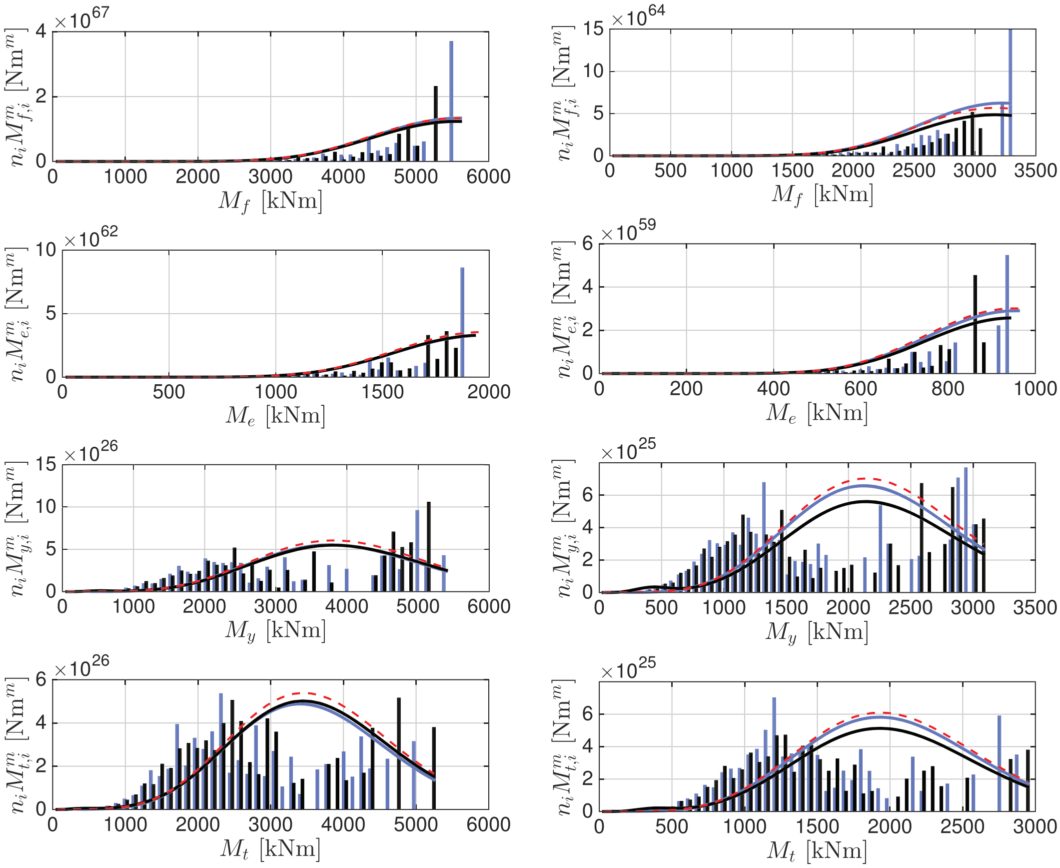

(A) $\lambda = 5.7$ (B) $\lambda = 7.55$

FIGURE 7 $\lambda = 5.7$ and 7.55: $n_i M_i^m$ for M_f, M_e, M_y, and M_t, for the AD-B (black bars and lines) and the VPM (blue bars and lines) approaches. The bars of the histogram are obtained using the RFC approach, while the distribution reported with the solid lines is computed using the DK method. The red dashed line corresponds to the distribution computed using the DK_{ext} procedure for the AD-B approach

4.5 | Extreme loads

To complete the analysis, we compare the extreme loads obtained using the VPM and the AD-B approaches for all the operating conditions and the considered moments. These loads are not expected to be representative of the highest ones the wind turbine components could meet during their lifetime. Indeed, with a TI of about 7%, the Mann turbulence field does not contain important wind changes. We also did not add a synthetic gust that could simulate an extreme wind event. We finally note that, for the above-rated condition ($\lambda = 5.7$), as the controller is inactive, the maximal loads are expected to be higher than those felt by a controlled turbine. However, the comparison of the maximal loads obtained in those simulations remains valuable in order to verify if the AD-B captures similar results as those of the VPM approach.

For each moment and operating conditions, we first estimate the maximal value of M_f and M_e obtained using the VPM method, for any blade, among all the turbulence boxes. The results are reported in Table 7. In order to perform consistent comparisons about the extreme loads, we consider two approaches for determining the maximal values in the AD-B results. As for the VPM method, we first determine the highest loads among all the turbulence boxes. The second value is evaluated as the maximum at approximately the same time and in the same turbulence box as those corresponding to the highest VPM loads. The differences between those AD-B values and the VPM highest loads are reported in Table 7.

The highest loads for M_f and M_e are similar for both VPM and AD-B results, whatever the method for computing the maximal value in the AD-B simulations. For the yaw and tilt moments, we observe more discrepancies, with differences varying between 2.4% and 25%. Although previous M_y and M_t statistics obtained using the AD-B method were in good agreement with those of the VPM results (see Sections 4.2–4.3), we here only compare one single value, and the errors can thus be high. In order to have a more relevant comparison for the extreme loads, and to investigate the accuracy of AD-B response to an extreme wind event, we should perform a simulation with a gust model. We leave this for further investigations.

10991824, 2022, 11, Downloaded from https://onlinelibrary.wiley.com/doi/10.1002/we.2772 by Bibliothecaire En Chef Uni Catholique De Louvain (Ucl), Wiley Online Library on [18/03/2024]. See the Terms and Conditions (https://onlinelibrary.wiley.com/terms-and-conditions) on Wiley Online Library for rules of use; OA articles are governed by the applicable Creative Commons License

10991824, 2022, 11, Downloaded from https://onlinelibrary.wiley.com/doi/10.1002/we.2772 by Bibliothecaire En Chef Uni Catholique De Louvain (Ucl), Wiley Online Library on [18/03/2024]. See the Terms and Conditions (https://onlinelibrary.wiley.com/terms-and-conditions) on Wiley Online Library for rules of use; OA articles are governed by the applicable Creative Commons License

TABLE 7 Maximal M_f, M_e, M_y, and M_t values for the VPM simulations and percentage difference between the AD-B and the VPM results

(a) M_f and M_e	VPM	AD-B$_{val,1}$	AD-B$_{val,2}$	VPM	AD-B$_{val,1}$	AD-B$_{val,2}$
λ	$M_{f,max}$ (kNm)	Difference (%)		$M_{e,max}$ (kNm)	Difference (%)	
5.7	8,530.13	0.47	−1.28	2,476.21	0.76	−3.22
7.55	8,348.58	2.02	0.53	1,415.47	1.17	−2.72
10.24	8,348.58	2.87	0.9	354.87	2.27	−2.17
(b) M_y and M_t						
λ	$\|M_{y,max}\|$ (kNm)	Difference (%)		$\|M_{t,max}\|$ (kNm)	Difference (%)	
5.7	2,820.39	−2.40	−2.40	2,736.50	13.67	13.67
7.55	1,519.66	13.08	−13.42	1,631.13	7.04	7.04
10.24	714.62	−2.36	−17.24	698.57	11.63	−24.50

5 | CONCLUSIONS

This work aimed at verifying the wind turbine fatigue loads and damages predicted by an advanced AD method coupled to LES, at a resolution similar to that used in large wind farm simulations. The strategy proposed in this study consisted of replicating blade trajectories through the disk and interpolate the AD aerodynamic forces onto these "virtual blades" at each time step.

This method, denoted AD-B, was verified with a higher fidelity approach at a finer resolution, a VPM method coupled to immersed LLs. We considered the NREL-5MW at three representative wind speeds and tip speed ratios and impacted by a turbulent wind.

The blade root bending moments and the rotor yaw and tilt moments were investigated. Two procedures were used for computing the cumulated damages and the equivalent moments: the rainflow counting method (RFC) and the Dirlik's approach (DK), both combined with a Palgrem–Miner rule. For both the AD-B and VPM methods, compared to the RFC method, the DK approach led to higher equivalent moments and damages. This was partly due to an incomplete upper tail of moment amplitudes for the RFC method, compared to the DK method that presented a "filled" distribution in those moment ranges. The differences were also aggravated by the moment signals that presented significant periodicity due to the blade rotation, for which the DK method was not originally defined. For both the RFC and DK procedures, the computed AD-B equivalent moments were close to those obtained using the VPM method, with a maximum difference of 4%. Depending on the material characteristics, those errors were more or less amplified in the cumulated damages (up to nearly 30%).

In this study, we also proposed to extrapolate the PSD of the moment fluctuations, used in the DK methodology. This aimed at modeling the AD-B behavior in the unresolved scales and decreasing the differences with respect to the VPM method. Globally, the use of the extrapolated PSDs made the AD-B fatigue estimates closer to those obtained using the VPM method, except for the lowest tip speed ratio. However, this study clearly highlighted that the contribution of the smallest moment amplitudes was negligible in the fatigue estimates: In fact, the results showed that the use of extrapolated PSDs changed the cycle number distribution in all the moment amplitudes and not only in the smallest ones. This was the change in the middle and large moment amplitudes that finally improved or degraded the performances of the AD-B approach.

Although further investigations about spectral counting methods and extrapolated PSDs should be interesting, the present study shows that the AD-B model combined with the RFC counting procedure produces M_{eq} that are very close to those obtained using the VPM method, without modeling any effect of the unresolved flow scales. Indeed, the AD-B approach at a coarse resolution already captures the flow scales that significantly impact the fatigue estimates. The methodology could be further improved with additional features (e.g., the inclusion of aeroelastic effects and gravitational loads,…). However, under the assumption of rigid blades, acceptable for wind turbines of reasonable size, and based on the conclusions of this paper, we expect an accurate estimation of the fatigue loads at a wind farm scale. Indeed, the addition of shear and wake effects, through the wake meandering in particular, mainly impacts the load cycles of medium and large amplitudes, which are well captured by the AD approach. In a similar way, the inclusion of the gravity, which mainly impacts the edgewise moments,[13] will affect cycles of large amplitudes, often higher than the ones related to the aerodynamic contributions (for the NREL-5MW in particular, this should be further confirmed for larger wind turbines). As the AD method captures well those load cycles, it seems reasonable to mention than the addition of the gravity should not decrease the performances of the AD method in the prediction of fatigue loads.

ACKNOWLEDGEMENTS

This project has received funding from the European Research Council (ERC) under the European Union's Horizon 2020 research and innovation program (grant agreement no. 725627). The simulations of one wind turbine using the actuator disk used computational resources provided by the Consortium des Équipements de Calcul Intensif (CÉCI), funded by the Fonds de la Recherche Scientifique de Belgique (F.R.S.-FNRS) under

Grant No. 2.5020.11. The other simulations used computational resources made available on the Tier-1 supercomputer of the Fédération Wallonie-Bruxelles, infrastructure funded by the Walloon Region under the Grant Agreement No. 1117545.

PEER REVIEW

The peer review history for this article is available at https://publons.com/publon/10.1002/we.2772.

ORCID

Maud Moens https://orcid.org/0000-0001-8374-4475
Philippe Chatelain https://orcid.org/0000-0001-9891-5265

REFERENCES

1. Sheng S. Report on wind turbine subsystem reliability-a survey of various databases (presentation). tech. rep., National Renewable Energy Lab.(NREL), Golden, CO (United States); 2013.
2. Dao C, Kazemtabrizi B, Crabtree C. Wind turbine reliability data review and impacts on levelised cost of energy. *Wind Energy*. 2019;22(12): 1848-1871. doi:10.1002/we.2404
3. Bossanyi EA. Individual blade pitch control for load reduction. *Wind Energy*. 2003;6(2):119-128.
4. Kallen T, Zierath J, Dickler S, Konrad T, Jassmann U, Abel D. Repetitive individual pitch control for load alleviation at variable rotor speed. *Journal of physics: Conference series*, Vol. 1618: IOP Publishing; 2020:22055.
5. Coquelet M, Bricteux L, Lejeune M, Chatelain P. Biomimetic individual pitch control for load alleviation. *J Phys Conf Ser*. 2020;1618(2):22052.
6. Kanev SK, Savenije FJ, Engels WP. Active wake control: An approach to optimize the lifetime operation of wind farms. *Wind Energy*. 2018;21(7): 488-501.
7. Capello E, Wada T, Punta E, Fujisaki Y. Trade-off between power extraction maximisation and fatigue reduction in wind farms via second-order sliding mode control and min–max optimisation. *IET Control Theory Appl*. 2020;14(17):2535-2547.
8. Bottasso CL, Cacciola S, Schreiber J. Local wind speed estimation, with application to wake impingement detection. *Renew Energy*. 2018;116:155-168. doi:10.1016/j.renene.2017.09.044
9. Aubrun S, Muller YA, Masson C. Predicting wake meandering in real-time through instantaneous measurements of wind turbine load fluctuations. *J Phys Conf Ser*. 2015;625:12005.
10. Muller Y-A, Aubrun S, Masson C. Determination of real-time predictors of the wind turbine wake meandering. *Exp Fluids*. 2015;56(3):53. doi:10.1007/s00348-015-1923-9
11. Lejeune M, Moens M, Coquelet M, Coudou N, Chatelain P. Data assimilation for the prediction of wake trajectories within wind farms. *J Phys Conf Ser*. 2020;1618(6):62055.
12. Bangga G, Lutz T. Aerodynamic modeling of wind turbine loads exposed to turbulent inflow and validation with experimental data. *Energy*. 2021;223: 120076. doi:10.1016/j.energy.2021.120076
13. Damiani R, Dana S, Annoni J, et al. Assessment of wind turbine component loads under yaw-offset conditions. *Wind Energy Sci*. 2018;3(1):173-189.
14. Madsen HA, Larsen TJ, Pirrung GR, Li A, Zahle F. Implementation of the blade element momentum model on a polar grid and its aeroelastic load impact. *Wind Energy Sci*. 2020;5(1):1-27.
15. Larsen TJ, Madsen HA, Larsen GC, Hansen KS. Validation of the dynamic wake meander model for loads and power production in the egmond aan zee wind farm. *Wind Energy*. 2013;16(4):605-624.
16. Larsen GC, Aagaard Madsen H, Bingöl F. Dynamic wake meandering modeling. Tech. Rep. Risø-R-1607 (EN), Risø National Laboratory; 2007.
17. Galinos C, Dimitrov N, Larsen TJ, Natarajan A, Hansen KS. Mapping wind farm loads and power production-a case study on horns rev 1. *J Phys Conf Ser*. 2016;753(3):32010.
18. Schmidt B, Lloyd G, Schmidt B, et al. Wake loads and fatigue load certification in offshore wind farms. In: Offshore EWEA Proceedings; 2011.
19. Harrison M, Bossanyi E, Ruisi R, Skeen N. An initial study into the potential of wind farm control to reduce fatigue loads and extend asset life. *J Phys Conf Ser*. 2020;1618(2):22007.
20. van Dijk MT, van Wingerden J-W, Ashuri T, Li Y. Wind farm multi-objective wake redirection for optimizing power production and loads. *Energy*. 2017;121:561-569. doi:10.1016/j.energy.2017.01.051
21. Riva R, Liew J, Friis-Møller M, et al. Wind farm layout optimization with load constraints using surrogate modelling. *J Phys Conf Ser*. 2020;1618(4): 42035.
22. Stanley APJ, King J, Ning A. Wind farm layout optimization with loads considerations. *Journal of Physics: Conference Series*, Vol. 1452: IOP Publishing; 2020:12072.
23. Lee S, Churchfield M, Driscoll F, et al. Load estimation of offshore wind turbines. *Energies*. 2018;11(7):1895.
24. Jonkman J, Buhl Jr M. FAST User's Guide. Tech. Rep., TP-500-38230, NREL, 2005.
25. Liu Z, Li Q, Ishihara T, Peng J. Numerical simulations of fatigue loads on wind turbines operating in wakes. *Wind Energy*. 2020;23(5):1301-1316.
26. Meng H, Li L, Zhang J. A preliminary numerical study of the wake effects on the fatigue load for wind farm based on elastic actuator line model. *Renew Energy*. 2020;162:788-801.
27. Churchfield MJ, Lee S, Moriarty PJ, et al. A comparison of the dynamic wake meandering model, large-eddy simulation, and field data at the egmond aan zee offshore wind plant. NREL/CP-5000-63321, National Renewable Energy Lab.(NREL); 2015.
28. Martínez-Tossas LA, Leonardi S. Wind turbine modeling for computational fluid dynamics. SR-5000-55054, NREL; 2013.
29. Wu Y-T, Porté-Agel F. Modeling turbine wakes and power losses within a wind farm using LES: An application to the Horns Rev offshore wind farm. *Renew Energy*. 2015;75:945-955. doi:10.1016/j.renene.2014.06.019
30. Moens M, Duponcheel M, Winckelmans G, Chatelain P. An actuator disk method with tip-loss correction based on local effective upstream velocities. *Wind Energy*. 2018;21(9):766-782.

10991824, 2022, 11, Downloaded from https://onlinelibrary.wiley.com/doi/10.1002/we.2772 by Bibliothecaire En Chef Uni Catholique De Louvain (Ucl), Wiley Online Library on [18/03/2024]. See the Terms and Conditions (https://onlinelibrary.wiley.com/terms-and-conditions) on Wiley Online Library for rules of use; OA articles are governed by the applicable Creative Commons License

31. Martinen S, Carlén I, Nilsson K, Breton S-P, Ivanell S. Analysis of the effect of curtailment on power and fatigue loads of two aligned wind turbines using an actuator disc approach. *J Phys Conf Ser*. 2014;524(1):012182.
32. ASTM AE. 1049–standard practices for cycle counting in fatigue analysis. West Conshohocken (PA); 2003.
33. Miner MA. Cumulative damage in fatigue. *J Appl Mech*. 1945;67:A159-A164.
34. Burton T, Jenkins N, Sharpe D, Bossanyi E. *Wind Energy Handbook*. England: John Wiley and Sons, Ltd; 2001.
35. Veers PS. Fatigue loading of wind turbines. *Wind energy systems*: Elsevier; 2011:130-158.
36. Ragan P, Manuel L. Comparing estimates of wind turbine fatigue loads using time-domain and spectral methods. *Wind Eng*. 2007;31(2):83-99.
37. Vera-Tudela L, Kühn M. Analysing wind turbine fatigue load prediction: The impact of wind farm flow conditions. *Renew Energy*. 2017;107:352-360.
38. Passipoularidis V, Brøndsted P. Fatigue evaluation algorithms: Review. 1740(EN), Denmark, Forskningscenter Risoe. Risoe-R, Danmarks Tekniske Universitet, Risø Nationallaboratoriet for Bæredygtig Energi; 2010.
39. Dirlik T. Application of computers in fatigue analysis. *Ph.D. Thesis*: Warwick University; 1985.
40. Halfpenny A. A frequency domain approach for fatigue life estimation from finite element analysis. *Key Eng Mater*. 1999;167:401-410.
41. Shan W. Gain scheduling pitch control for fatigue load reduction for wind turbines. *Ph.D. Thesis*: Fraunhofer Institute for Wind Energy and Energy System Technology (IWES), Kassel; 2015.
42. Shan M. Load reducing control for wind turbines: load estimation and higher level controller tuning based on disturbance spectra and linear. *Ph.D. Thesis*: University of Kassel; 2017.
43. Duponcheel M, Bricteux L, Manconi M, Winckelmans G, Bartosiewicz Y. Assessment of RANS and improved near-wall modeling for forced convection at low Prandtl numbers based on LES up to $Re_\tau = 2000$. *Int J Heat Mass Transfer*. 2014;75:470-482. doi:10.1016/j.ijheatmasstransfer.2014.03.080
44. Winckelmans GS, Jeanmart H. Assessment of some models for les without/with explicit filtering. In: Geurts BJ, Friedrich R, Métais O, eds. *Direct and large-eddy simulation iv*. Dordrecht: Springer Netherlands; 2001:55-66.
45. Smagorinsky J. General circulation experiments with the primitive equations. *Mon Weather Rev*. 1963;91(3):99-164.
46. Monaghan JJ. Extrapolating B splines for interpolation. *J Comput Phys*. 1985;60(2):253-262. doi:10.1016/0021-9991(85)90006-3
47. Chatelain P, Backaert S, Winckelmans G, Kern S. Large eddy simulation of wind turbine wakes. In: Rodi W, ed. *Proceedings of the 9th international symposium on engineering turbulence modelling and measurements (ETMM-9), june 6–8, 2012, Thessaloniki, Greece*, Flow, Turbulence and Combustion: Springer; 2013:587-605.
48. Chatelain P, Duponcheel M, Caprace DG, Marichal Y, Winckelmans G. Vortex particle-mesh simulations of vertical axis wind turbine flows: from the airfoil performance to the very far wake. *Wind Energy Sci*. 2017;2(1):317-328. doi:10.5194/wes-2-317-2017
49. Caprace D-G, Chatelain P, Winckelmans G. Wakes of rotorcraft in advancing flight: a large-eddy simulation study. *Phys Fluids*. 2020;32(8):087107.
50. Balty P, Caprace D-G, Waucquez J, Coquelet M, Chatelain P. *Multiphysics Simulations of the Dynamic and Wakes of a Floating Vertical Axis Wind Turbine*, Vol. 1618: IOP Publishing; 2020;062053.
51. Moens M, Coquelet M, Trigaux F, Chatelain P. Handling individual pitch control within an actuator disk framework: Verification against the actuator line method and application to wake interaction problems. accepted for publication in Journal of Physics: Conference Series; 2022.
52. Trigaux F, Chatelain P, Winckelmans G. A flexible actuator curve model for aeroelastic simulationsof wind turbines in atmospheric boundary layers. accepted for publication in Journal of Physics: Conference Series; 2022.
53. Goodman J. *Mechanics applied to engineering*: Longmans, Green; 1919.
54. Mandell JF, Samborsky DD. *Doe/msu Composite Material Fatigue Database: Test Methods, Materials, and Analysis*: Sandia National Laboratories Albuquerque; 1997.
55. Jonkman J, Butterfield S, Musial W, Scott G. Definition of a 5-MW Reference Wind Turbine for Offshore System Development. TP-500-38060, NREL; 2009.
56. AWEA, BlueGreen, GLWN, NIST. Wind energy industry manufacturing supplier handbook, USA, AWEA; 2011.
57. Guideline GW, Lloyd G. Guideline for the certification of wind turbines, Hamburg: Germanischer Lloyd Wind Energie Gmb H; 2010.
58. Shipley DE, Miller MS, Robinson MC. Dynamic stall occurrence on a horizontal axis wind turbine blade. TP-442-6912, National Renewable Energy Lab.(NREL), Golden, CO (United States); 1995.
59. Hansen MH, Gaunaa M, Aagaard Madsen H. A beddoes-leishman type dynamic stall model in state-space and indicial formulations [wind turbines]. RISO-R-1354, Risoe National Lab., Roskilde (Denmark). Wind Energy Dept.; 2004.
60. Leishman GJ. *Principles of Helicopter Aerodynamics*. 2nd ed.: Cambridge University Press; 2006.
61. Mann J. Wind field simulation. *Probabilistic Eng Mech*. 1998;13(4):269-282. doi:10.1016/S0266-8920(97)00036-2
62. Moriarty PJ, Holley WE, Butterfield SP. Extrapolation of extreme and fatigue loads using probabilistic methods. TP-500-34421, National Renewable Energy Lab., Golden, CO (US); 2004.

How to cite this article: Moens M, Duponcheel M, Chatelain P. Assessment of an actuator disk-based approach for the prediction of fatigue loads in a perspective of wind farm-scale application. *Wind Energy*. 2022;25(11):1860-1879. doi:10.1002/we.2772

10991824, 2022, 11, Downloaded from https://onlinelibrary.wiley.com/doi/10.1002/we.2772 by Bibliothecaire En Chef Uni Catholique De Louvain (Ucl), Wiley Online Library on [18/03/2024]. See the Terms and Conditions (https://onlinelibrary.wiley.com/terms-and-conditions) on Wiley Online Library for rules of use; OA articles are governed by the applicable Creative Commons License